

## MIT Open Access Articles

*Viscous entrainment on hairy surfaces*

The MIT Faculty has made this article openly available. **Please share** how this access benefits you. Your story matters.

**Citation:** Nasto, Alice et al. "Viscous entrainment on hairy surfaces." *Physical Review Fluids* 3, 2: 024002 © 2018 American Physical Society

**As Published:** <http://dx.doi.org/10.1103/PhysRevFluids.3.024002>

**Publisher:** American Physical Society

**Persistent URL:** <http://hdl.handle.net/1721.1/114296>

**Version:** Final published version: final published article, as it appeared in a journal, conference proceedings, or other formally published context

**Terms of Use:** Article is made available in accordance with the publisher's policy and may be subject to US copyright law. Please refer to the publisher's site for terms of use.



## Viscous entrainment on hairy surfaces

Alice Nasto,<sup>1</sup> P.-T. Brun,<sup>2</sup> and A. E. Hosoi<sup>1,2</sup>

<sup>1</sup>*Department of Mechanical Engineering, Massachusetts Institute of Technology,  
Cambridge, Massachusetts 02139, USA*

<sup>2</sup>*Department of Mathematics, Massachusetts Institute of Technology,  
Cambridge, Massachusetts 02139, USA*



(Received 6 July 2017; published 7 February 2018)

Nectar-drinking bats and honeybees have tongues covered with hairlike structures, enhancing their ability to take up viscous nectar by dipping. Using a combination of model experiments and theory, we explore the physical mechanisms that govern viscous entrainment in a hairy texture. Hairy surfaces are fabricated using laser cut molds and casting samples with polydimethylsiloxane (PDMS) elastomer. We model the liquid trapped within the texture using a Darcy-Brinkmann-like approach and derive the drainage flow solution. The amount of fluid that is entrained is dependent on the viscosity of the fluid, the density of the hairs, and the withdrawal speed. Both experiments and theory reveal an optimal hair density to maximize fluid uptake.

DOI: [10.1103/PhysRevFluids.3.024002](https://doi.org/10.1103/PhysRevFluids.3.024002)

### I. INTRODUCTION

There has been a significant effort to rationalize drinking strategies in nature through the lens of fluid mechanics. Animals take advantage of the physical mechanisms available at different scales. For example, capillary forces play a key role in nectar uptake by hummingbirds, who use elastocapillarity to fold their tongues into tubes to draw up nectar [1,2]. Phalaropes use contact angle hysteresis to bring drops of water from the tips of their beaks to their mouths through a scissoring motion [1]. Cats set the frequency of their lapping motion through a competition between gravity and inertia [3]. Viscous dipping is a method utilized by many nectar-drinking animals, whereby fluid is viscously entrained on the surface of a tongue [1,4,5]. This mechanism is reminiscent of Landau-Levich-Derjaguin (LLD) dip coating and has been analyzed through this framework [4,6,7]. Viscous coatings on tongues are also relevant in the context of prey capture, such as by chameleons [8].

Many viscous dipping animals have hairlike structures on their tongues [5,9–11]; however, the effect of this texture has not been considered in viscous dipping models [1,4]. In this study, we are motivated by nectar-drinking bats, such as *Glossophaga soricina*, who feed via viscous dipping with tongues covered in hairlike papillae [5]. A schematic illustrating the drinking mechanism is shown in Fig. 1. These papillae contain blood vessels which become engorged with blood during tongue retraction, causing the papillae to stand erect, increasing nectar uptake [5]. Honeybees use a tension mechanism to erect hairs on its tonguelike glossa during nectar feeding [9,10]. Inspired by this observation, we explore the impact of hairy textures on viscous entrainment.

Previous work has investigated the effect of microscale texture on dip coating [12]. Seiwert *et al.* model entrainment by modifying the LLD theory for a two-layer film consisting of a layer of liquid trapped within the texture and a free film on top of the texture [12]. Here, we instead investigate textures at a mesoscale, namely, a millimetric scale that is an intermediary between a microscale and what is typically thought of as a large scale. We begin by conducting model experiments with hairy textured surfaces withdrawn from fluid baths.

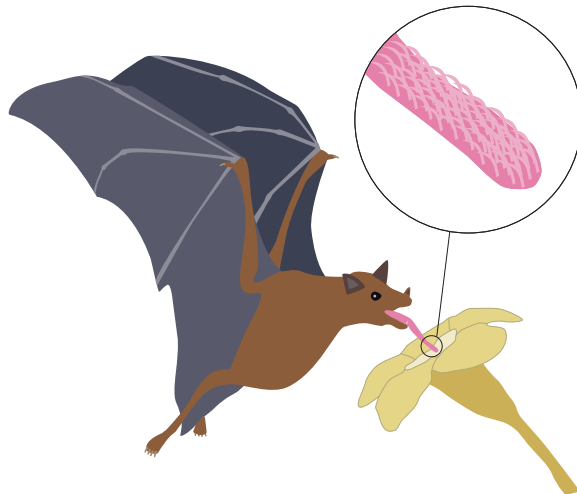


FIG. 1. Illustration of a bat drinking nectar. The inset shows the hairlike texture of the papillae that cover the tongue.

## II. EXPERIMENTAL SETUP

Hairy surfaces [shown in Fig. 2(a)] are cast from polydimethylsiloxane (PDMS) elastomer (with Young's modulus  $E = 2$  MPa) using laser cut acrylic molds. The hairs are shaped like truncated cones with an average diameter of  $e = 0.3$  mm and a length of  $l = 2.7$  mm. The hairs are arranged in a hexagonal pattern with an edge-to-edge spacing  $r$  ranging from  $r = 0.2$  mm to  $r = 4.2$  mm [shown in Fig. 2(b)]. The hairy surfaces are  $W = 40$  mm wide and  $L = 60$  mm long.

The hairy surfaces are plunged into silicone oil at a sufficiently low speed ( $V_{\text{plunge}} = 0.5$  m/s) so as to avoid air entrainment [13]. After the sample is fully submerged, it is withdrawn from a bath of silicone oil at speed  $V$  until the sample has fully exited the bath; then the sample is held stationary.

Figure 2(c) shows a time series of images from an experiment in which a hairy sample with hair spacing  $r = 2.2$  mm is withdrawn from a bath of silicone oil with viscosity  $\nu = 1000$  cSt at a speed  $V = 40$  mm/s. The red solid line is drawn at the base of the hairs and the red dashed line is drawn over the profile of the liquid. Liquid fills the hairs to their tips as it exits the bath ( $t \leq 1.5$  s). Over time, the liquid drains. The profile of the fluid within the hairy texture has two regions: The bottom region where the spaces between hairs are completely filled and the thickness is uniform, which is separated by a drainage front from the top region where the film is thinning. The position of the drainage front is indicated with blue triangles in Fig. 2(c).

Figure 3(a) shows snapshots of hairy surfaces of various hair densities at the moment that they fully exit the bath for withdrawal speed  $V = 40$  mm/s. For high hair densities, such as  $r = 0.2$  or  $r = 0.7$  mm, the hairy surfaces emerge with the hairs fully filled to their tips with fluid and an additional thin film topping the hairs. For intermediate densities, such as  $r = 2.2$  mm, the hairs are filled to the tips of the hairs as they emerge from the bath, but the liquid drains to a visible extent from the top hairs before the sample fully exits. For low densities, such as  $r = 4.2$  mm, the liquid coating does not reach the level of the tips of the hairs.

We measure the mass of the fluid taken up in hairy textures of various edge-to-edge hair spacing  $r$  at the moment they fully exit a silicone oil bath with various viscosities  $\nu$  at various withdrawal speeds  $V$ . The mass is measured using a material testing machine with a load cell and a motorized linear stage. The sample is hairy on one side and untextured on the opposite side; measurements with identical conditions are taken with untextured samples and are used to correct the measurements on the hairy samples so as to measure only the mass of the fluid taken up on the hairy side of the sample. For each data point, the experiment is repeated five times and the reported data are an average with

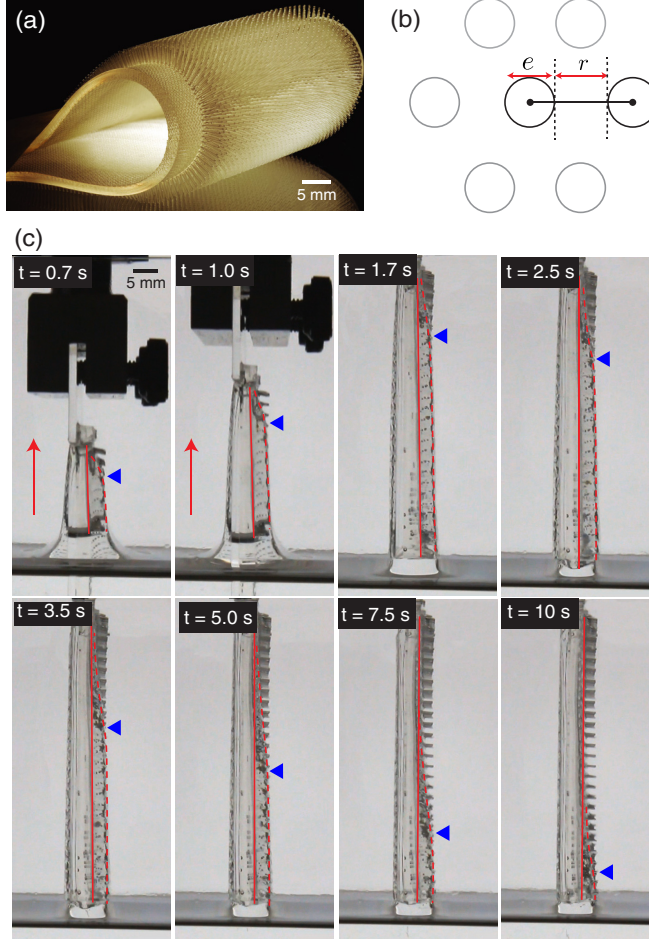


FIG. 2. (a) Hairy surfaces made from laser cut molds and cast using PDMS elastomer. (Photo credit Felice Frankel.) (b) Schematic illustrating arrangement and spacing of hairs in a triangular lattice. (c) Time series of images from an experiment with hairs of  $r = 2.2$  mm being pulled out of  $\nu = 1000$  cSt silicone oil at a speed of  $V = 40$  mm/s. The red solid line is drawn at the base of the hairs and the red dashed line is drawn over the profile of the liquid. The red arrows indicate frames in which the sample is emerging from the liquid. The blue triangles point to the position of the drainage front.

the error bar reporting the standard deviation. The experimental measurements of mass taken up versus the edge-to-edge spacing of the hairs  $r$  are plotted in Fig. 3(b). The different colored curves correspond to different withdrawal velocities and the different symbol shapes correspond to different viscosities. The amount of fluid taken up increases with the withdrawal velocity and viscosity. The curves corresponding to experiments with three different viscosities are separated into three distinct regions [shaded in different levels of gray in the Fig. 3(b)]. Note that there is an optimal hair spacing to maximize fluid uptake which we relate to the spacing of the hairs and the drainage of the fluid between the hairs in the following sections.

### III. MODEL

The drainage of the fluid diminishes the amount of fluid that is taken up. To account for the drainage, we use a Darcy-Brinkmann model for a porous medium near a solid boundary. In this

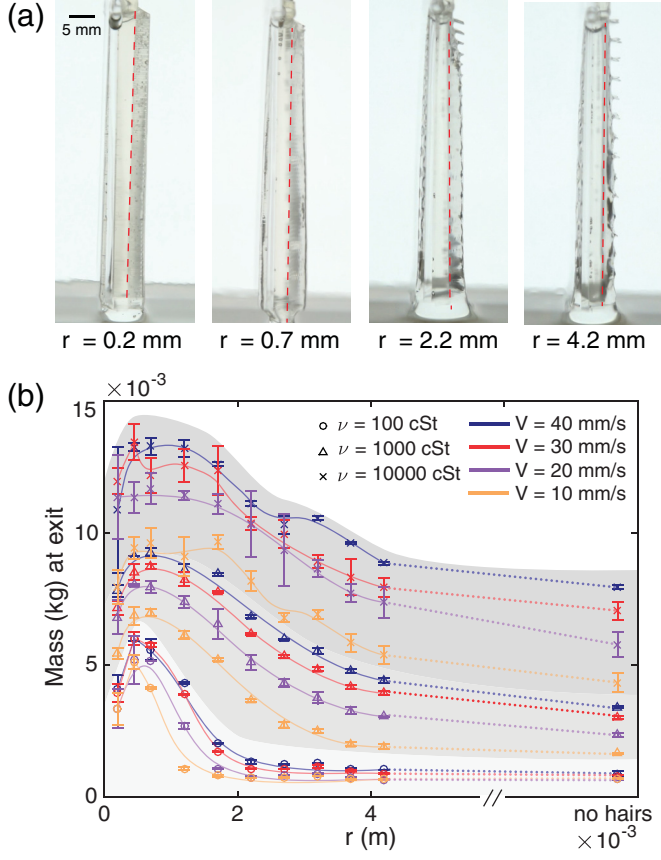


FIG. 3. (a) Images of hairy samples of different hair spacing  $r$  for withdrawal speed  $V = 40$  mm/s at the moment the samples fully exit the bath. (b) Weight of liquid coating the hairy side of the plate vs the center-to-center spacing of the hairs  $r$  for various withdrawal speeds  $V$  and viscosities  $\nu$ .

model, the columns of hair are treated as channels with the hairs acting as walls (see Fig. 4); this leads to dissipation along the width of the effective channel due to the presence of these walls. Taking advantage of the geometry of the problem, we define the flow profile along a groove of rectangular cross section,

$$\mathbf{u} = \bar{\mathbf{u}}(x, z) \frac{6y}{h_{\text{eff}}^2} (h_{\text{eff}} - y), \quad (1)$$

where  $h_{\text{eff}}$  is the effective channel width and  $\bar{\mathbf{u}} = (u, v)$  is the flow velocity in the  $x$ - $z$  plane. Later we show that  $h_{\text{eff}}$  for the hairy surfaces is the edge-to-edge hair spacing  $r$ . This expression is valid for  $0 < y < h_{\text{eff}}$  and constitutes a building block of the flow. The flow in the sample is seen as a collection of such units stacked along the  $y$  direction. In each block, the flow in the  $y$  direction is a parabola and the three-dimensional Stokes equation may be reduced to the Brinkmann equation

$$\nu(\bar{\nabla}^2 \bar{\mathbf{u}} - k^2 \bar{\mathbf{u}}) - \frac{1}{\rho} \bar{\nabla} p + \mathbf{g} = \mathbf{0}, \quad (2)$$

where  $k = \sqrt{12}/h_{\text{eff}}$ ,  $\mu$  is the fluid's kinematic viscosity,  $\rho$  is its density,  $\mathbf{g}$  is the acceleration of gravity, and an overbar denotes an operator that is constrained to the  $x$ - $z$  plane. When the hair spacing is much smaller than the other length scales of the problem we anticipate the prevalence of

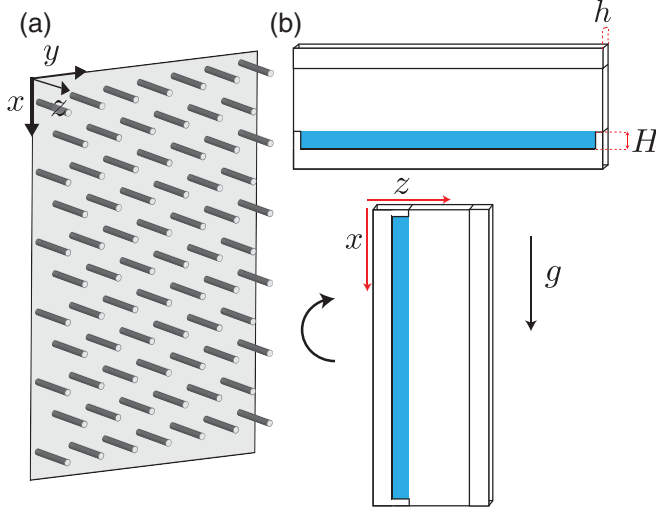


FIG. 4. (a) Schematic of the hairy sample with a coordinate system corresponding to the Hele-Shaw-style experiment. (b) Schematic demonstrating Hele-Shaw-style experimental setup. The cell is filled horizontally with a film of a target initial height. The cell is then placed in a vertical position so that the film drains.

$k^2$  in viscous effects. Equation (2) may now be used to define a drainage speed using the lubrication approximation [14], i.e.,  $v \ll u$ , and characteristic variations in the  $z$  direction are much smaller than characteristic variations in the  $x$  direction. Projecting Eq. (2) along the  $z$  direction, we find that the pressure is everywhere prescribed by the Laplace law  $p(x, t) = p_a + \gamma\kappa$ , where  $p_a$  is the atmospheric pressure,  $\gamma$  the fluid interfacial tension, and  $\kappa$  the interface curvature. As a first approximation we assume that the interface curvature remains negligible so that  $p \simeq p_a$  and Eq. (2) yields

$$v \left( \frac{\partial^2 u}{\partial z^2} - \frac{12}{h_{\text{eff}}^2} u \right) = -g, \quad (3)$$

subject to the no-slip boundary condition at the bottom and vanishing stresses at the free surface. The solution of this equation is

$$u(z) = V_{\text{drain}} \left[ 1 - \cosh \left( \frac{2\sqrt{3}(l-z)}{h_{\text{eff}}} \right) \text{sech} \left( \frac{2\sqrt{3}l}{h_{\text{eff}}} \right) \right], \quad (4)$$

with

$$V_{\text{drain}} = \frac{gh_{\text{eff}}^2}{12\nu}. \quad (5)$$

In the limit of  $l \gg h_{\text{eff}}$  we find that the flow profile is nearly uniform with speed  $V_{\text{drain}}$ , aside from a boundary layer near the base of the hair and whose size scales like  $h_{\text{eff}}$ . This result could have been anticipated owing to the structure of Eq. (3), where the term in  $h_{\text{eff}}^2$  dominates the other source of viscous dissipation so that this ordinary differential equation is effectively an algebraic equation. We therefore predict that the drainage speed is independent of the height  $H$  of the fluid provided the fluid height does not exceed the length of the hairs. This finding is in stark contrast to the classical drainage solution, in which the front speed depends on the fluid height squared [14].

To measure the shape of the drainage front as predicted from our model, we consider a model experiment that mimics the flow between two adjacent rows of hairs [shown in Fig. 4(a)], which we treat as flow through a channel. The simplified model system is reminiscent of a Hele-Shaw cell and has two glass plates sandwiched together with shims of thickness  $h$ . A schematic of this setup is

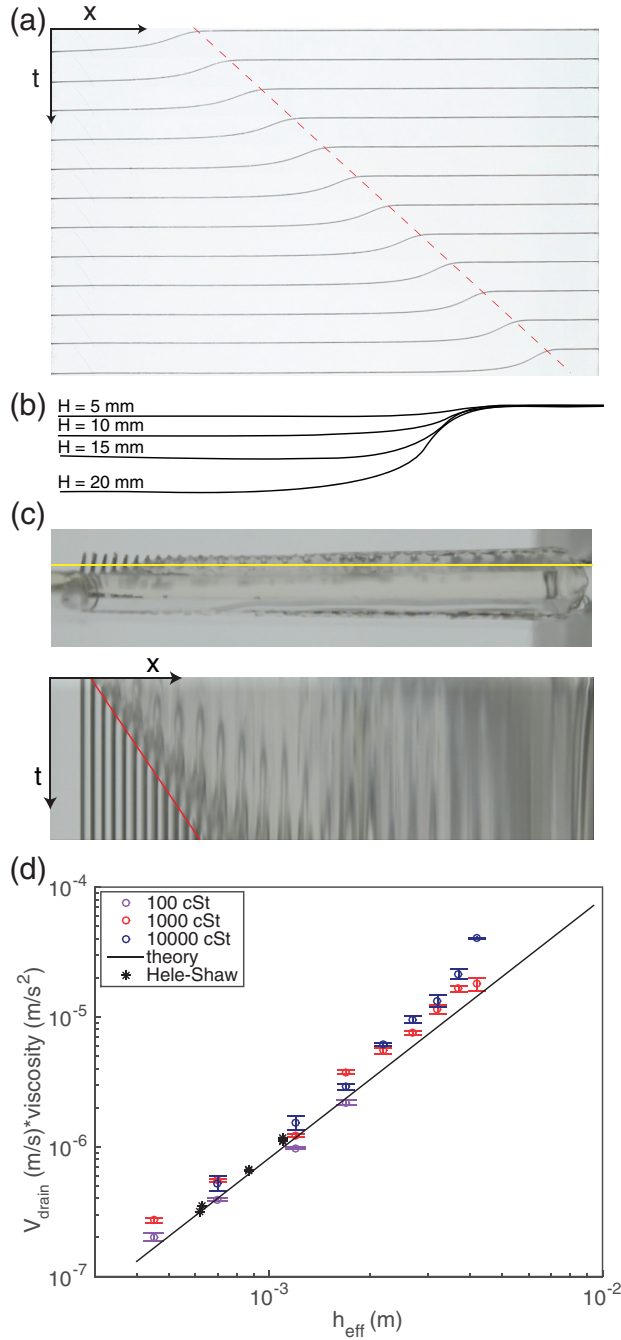


FIG. 5. (a) Experimental images showing the time series of the drainage front for  $\nu = 1000$  cSt, a gap size of  $h = 1$  mm, and an initial film height of  $H = 10$  mm. Snapshots are taken over consecutive 10-s intervals. (b) Experimentally measured profiles of drainage fronts for varying initial gap heights from  $H = 5$  mm to  $H = 25$  mm. (c) Kymograph with one-pixel slices from each frame of a video of a liquid draining from a hairy sample (shown sample is with  $r = 0.7$  mm and  $\nu = 1000$  cSt silicone oil). The yellow line indicates where the pixel slice is taken from each frame. The red line traces the drainage front as it progresses in the frames and the slope is used to measure the front speed. (d) Drainage speed vs  $h_{\text{eff}}$ , the effective channel width.



shown in Fig. 4(b). The cell is filled horizontally so that the film has a uniform initial height  $H$ . Then the cell is rotated  $90^\circ$  to a vertical position and the drainage is observed. A time series of images from a representative experiment with oil viscosity  $\nu = 1000$  cSt and a gap size of  $h = 1$  mm is shown in Fig. 5(a). The drainage front is sigmoidal in shape and translates down the cell as it moves.

Additionally, we investigate the effect of changing the initial height of the film  $H$ , which corresponds to the length of the hairs. Overlapped snapshots of the shape of the films draining from experiments with four different initial film heights taken at the same time are shown in Fig. 5(b). We find that the speed of the drainage front is unaffected by the initial film height.

We compare the Hele-Shaw system to the hairy samples by using experimental measurements of the fluid drainage speeds for both experiments so that we can relate the gap size between the plates to the effective spacing of the hairs. The fluid drainage speed is measured using a kymograph (a spatiotemporal diagram) with vertical slices from video frames that are one pixel wide passing through the center of the liquid film [an example is shown in Fig. 5(c)]. The slices from each frame are placed on top of one another in a single image with time increasing from top to bottom. A line can be traced in the kymograph over the moving drainage front, showing that the front speed is constant [an example with a red line drawn over the moving drainage front is shown in Fig. 5(c)]. The slope of the line is used to obtain the speed. For the experiments on hairy surfaces, the samples are withdrawn from the bath at a speed of  $V = 40$  mm/s (the upper limit that the apparatus allows) and the drainage front is tracked starting from the moment that the sample fully exits the bath and is held stationary. The fastest possible withdrawal speed is chosen to maximize the fluid taken up to be able to observe the drainage for the longest possible time. However, the withdrawal speed does not have an effect on the drainage front speed. Figure 5(d) shows the drainage speed multiplied by the viscosity for Hele-Shaw and hairy sample experiments versus  $h_{\text{eff}}$ , where  $h_{\text{eff}}$  is the space between plates  $h$  for the Hele-Shaw experiments and  $r$ , the edge-to-edge spacing between hairs, for the hairy sample experiments. The curves from these two types of experiments collapse on one another, showing that the Hele-Shaw experiments are a good model for the hairs and that the drainage flow between the hairs spaced at a distance  $h$  apart is equivalent to the drainage flow in a hairy sample where hairs are spaced at an equivalent distance  $h = r$ . The line in Fig. 5(d) corresponds to the theory and has a slope of 2 and a prefactor of  $g/12$ . Note that the very last few points of the plot (large  $h_{\text{eff}}$ ) deviate from our theory. For those experiments, the spacing between hairs is large enough such that Darcy-Brinkmann assumptions begin to break down.

#### IV. DISCUSSION

The amount of fluid taken up by the hairy surface at the moment it exits the bath is defined as the amount initially taken up, minus the volume that drained during the retraction time. Based on our experimental observations, we assume that the initial film coating the surface is approximately as thick as the hairs are long (valid for  $\nu = 100$  cSt for dense hairs  $r \leq 2.2$  mm and for  $\nu = 1000$  cSt for densities  $1.7 \text{ mm} \leq r \leq 3.2 \text{ mm}$ ). The expression for the mass of the fluid at the time  $t = L/V$ , as the hairy surface fully exits the bath, is modeled as the amount of fluid trapped in between the hairs minus the volume that has flown as the surface is pulled out of the bath. Assuming the fluid fills the hair up to its tip, we note that, in the absence of drainage, the uptake of fluid is

$$M_{\text{full}} = \rho W L l \left( 1 - \frac{\pi e^2}{2\sqrt{3}(e+r)^2} \right). \quad (6)$$

The second term in large parentheses accounts for the volume occupied by the hairs arranged in a hexagonal lattice. The flow profile in Eq. (4) is nearly uniform with amplitude  $V_{\text{drain}}$ , so the mass  $M_{\text{drain}}$  lost by drainage is

$$M_{\text{drain}} = \rho W l \int_0^{L/V} V_{\text{drain}} dt = \rho W l V_{\text{drain}} \frac{L}{V} \quad (7)$$



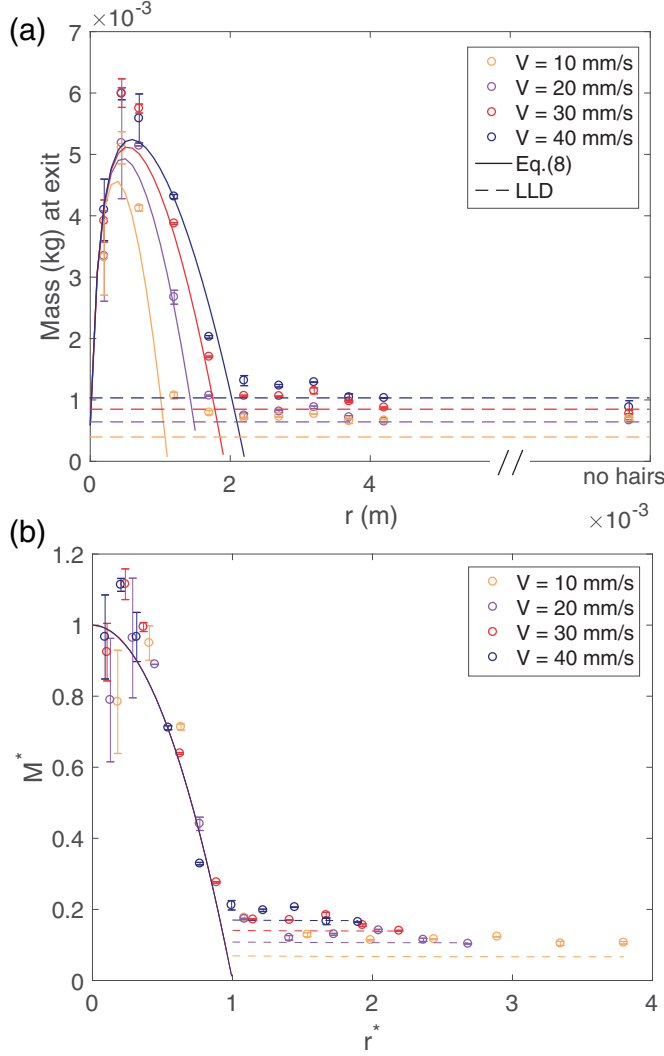


FIG. 6. (a) Mass of fluid taken up by the hairs measured at the time when the surface fully exits the bath vs  $r$  for experiments with silicone oil of viscosity  $\nu = 100$  cSt for various withdrawal speeds  $V$ . The solid lines are the mass as calculated from the theory from Eq. (8). The dashed lines are the mass as calculated according to LLD theory for dip coating of untextured surfaces. (b) Nondimensionalized experimental data from experiments with silicone oil of viscosity  $\nu = 100$  cSt. The solid lines correspond to the nondimensionalized mass as calculated from the theory from Eq. (8). The dashed lines are the nondimensionalized mass as calculated according to LLD theory [6,7].

and we conclude that

$$M = M_{\text{full}} \left( 1 - \frac{gr^2}{12\nu V} \right). \quad (8)$$

We define  $r_{\text{limit}} = \sqrt{12\nu V/g}$  as the spacing for which the drainage matches the retraction speed [see Eq. (5)]. As  $r$  approaches  $r_{\text{limit}}$ , the mass  $M$  approaches zero. In Fig. 6(a) we plot the measured mass from experimental data for hairs pulled from  $\nu = 100$  cSt silicone oil at various speeds. The solid lines are the mass  $M$  from Eq. (8) vs  $r$  for various  $V$ . In both data and theory,  $M$  is found to have

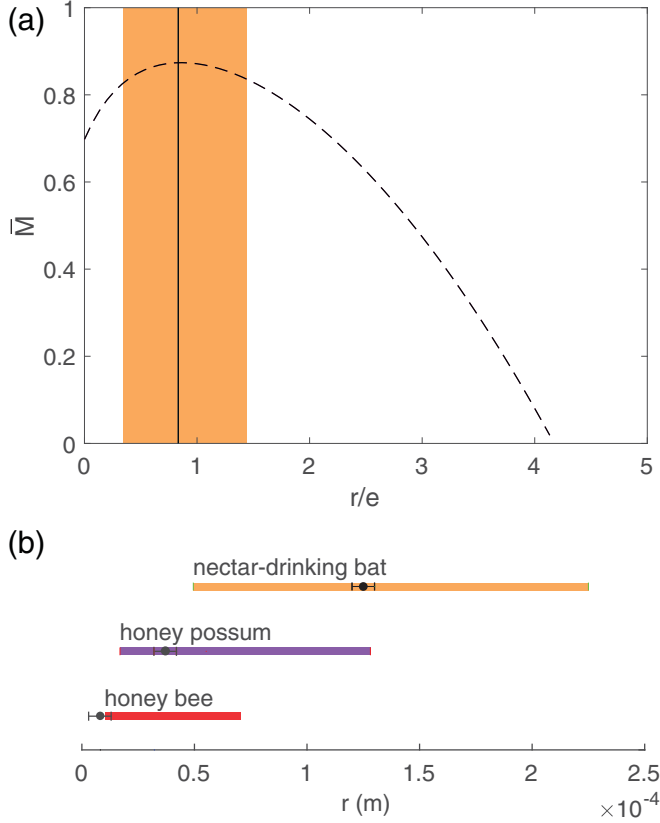


FIG. 7. (a) Theoretical mass of the fluid at the exit as calculated using the bat parameters vs  $r$ . The vertical line is the value of  $r$  that corresponds to physiological bat data. The orange region indicates values of  $M$  within 95% of the maximum. (b) Measured edge-to-edge spacing  $r$ , represented by black dots and horizontal error bars corresponding to uncertainties in measuring the spacing of the hairs, for three different nectar-drinking animals. The spacing  $r_{\max}$  that maximizes the mass of the fluid taken up is calculated using parameters for three different animals and Eq. (8). The color horizontal bars represent the range of  $r$  within 95% of the maximum value of  $M$ .

a maximum, and the theoretical value for  $r$  that maximizes the mass intake is consistent with our experiments. This optimum combines two competing effects: Denser hairs lead to slower drainage, but the volume available for liquid to be trapped diminishes as the hair spacing approaches zero (i.e., the limit of a solid wall). Additionally, we plot dashed horizontal lines corresponding to what is predicted by LLD dip coating of untextured plates pulled out at different speeds. According to LLD theory, the thickness  $h$  on an untextured surface pulled from a bath at speed  $V$  is  $h \simeq 0.94\ell_c \text{Ca}^{2/3}$ , where  $\ell_c = \sqrt{\sigma/\rho g}$  is the capillary length and  $\text{Ca} = \mu V/\sigma$  is the capillary number, with  $\sigma$  the air-liquid surface tension [6,7]. The LLD theory agrees well for large values of  $r$ ; the coating of surfaces with sparse hairs is as if the fluid is coating an untextured surface.

To unify our observations, we plot the experimental data in a dimensionless form in Fig. 6(b). The mass  $M$  is made dimensionless with  $M^* = M/\rho V_{\text{space}}$ , where  $V_{\text{space}}$  is the volume of the space between hairs. To nondimensionalize the spacing radius  $r$ , we define a characteristic length scale  $R_{\text{char}}^2 = 12\nu V/g$  and define  $r^* = r/R_{\text{char}}$ . Plotted in this nondimensional form, the theory curves corresponding to the various withdrawal speeds  $V$  and the experimental data collapse onto a single curve. The dashed lines corresponding to nondimensionalized LLD theory agree with the  $r^* > 1$  data. With these results in hand, we turn back to our initial motivation, bat drinking strategies.

Using the parameters from the physiology of *Glossophaga soricina* bat tongues and the measured speed of their drinking from Harper *et al.* [5], we apply our theory to place bat drinking in the context of our model system. The bats have conical hairs with a base diameter  $e \approx 0.15$  mm that are spaced at a edge-to-edge distance  $r \approx 0.125$  mm. The sucrose solution in the bat experiments has a 17% mass to mass concentration, which has a viscosity of  $\nu \approx 2$  cSt [15]. The ratio of the drainage speed to the withdrawal speed for bats is  $V_{\text{drain}}/V = 17.4$ , which lies within the range of speed ratios for our experiments,  $0.1 \gtrsim V_{\text{drain}}/V \gtrsim 1000$ . In Fig. 7(a) we plot the uptake efficiency  $\bar{M} = M/\rho W L l$  of liquid taken up by the tongue vs  $r/e$ . The value of  $r/e$  that corresponds to bat tongue physiological measurements is plotted as a vertical line. In the theory curve, the maximum occurs at  $r_{\text{max}} = 0.13$  mm. For bats,  $r \approx 0.125$  mm and lies within the region of the curve that is 95% of the maximum value [shaded in orange in Fig. 7(a)]. In this regime, the average thickness of the fluid layer entrained in the hairs is roughly 1 mm, ten times larger than what is attainable for an untextured surface [6,7], suggesting that there is a significant benefit to having hairs for taking up nectar.

Note, however, the limitations of our model, which assumes that the hairs lie on a planar substrate. In reality, the hairy surface is wrapped around a round bat tongue. Nevertheless our results indicate that the physical mechanism we have described is robust. Using data for three different animals, honeybees (*Apis mellifera ligustica*) [16], honey possums (*Tarsipes rostratus*) [11], and nectar-drinking bats (*Glossophaga soricina*), we calculate the theoretical spacing  $r_{\text{max}}$  maximizing the uptake in Eq. (8). In Fig. 7(b) we compare the theoretical values for  $r_{\text{max}}$  and the actual spacing  $r$  for these three different animals. The measured edge-to-edge spacing  $r$  is represented by black dots, with horizontal error bars corresponding to uncertainties in measuring the spacing of the hairs. The spacing  $r_{\text{max}}$  that maximizes the mass of the fluid taken up is calculated using parameters for three different animals and Eq. (8). The color horizontal bars represent the range of  $r$  within 95% of the maximum value of  $\bar{M}$ . We note that for very small textures, such as the hairs on bee tongues, surface tension plays a dominant role, which would make wicking an important mechanism to consider at this scale [17]. Additionally, we anticipate that other fluid-structure mechanisms come into play for expelling the trapped fluid at the end of the drinking cycle.

## ACKNOWLEDGMENT

A.N. and A.E.H. acknowledge support from the US Army Research Office under Grant No. ARO W911NF-15-1-0166.

- 
- [1] W. Kim and J. W. M. Bush, Natural drinking strategies, *J. Fluid Mech.* **705**, 7 (2012).
  - [2] W. Kim, F. Peaudecerf, M. W. Baldwin, and J. W. M. Bush, The hummingbird’s tongue: A self-assembling capillary syphon, *Proc. R. Soc. B* **279**, 4990 (2012).
  - [3] P. M. Reis, S. Jung, J. M. Aristoff, and R. Stocker, How cats lap: Water uptake by *Felis catus*, *Science* **330**, 1231 (2010).
  - [4] W. Kim, T. Gilet, and J. W. M. Bush, Optimal concentrations in nectar feeding, *Proc. Natl. Acad. Sci. USA* **108**, 16618 (2011).
  - [5] C. J. Harper, S. M. Swartz, and E. L. Brainerd, Specialized bat tongue is a hemodynamic nectar mop, *Proc. Natl. Acad. Sci. USA* **110**, 8852 (2013).
  - [6] L. Landau and B. Levich, Dragging of a liquid by a moving plate, *Acta Physicochim. URSS* **17**, 42 (1942).
  - [7] B. Derjaguin, On the thickness of the liquid film adhering to the walls of a vessel after emptying, *Prog. Surf. Sci.* **43**, 134 (1993).
  - [8] F. Brau, D. Lanterbecq, L.-N. Zghikh, V. Bels, and P. Damman, Dynamics of prey prehension by chameleons through viscous adhesion, *Nat. Phys.* **12**, 931 (2016).

- [9] H. Yang, J. Wu, and S. Yan, Effects of erectable glossal hairs on a honeybee's nectar-drinking strategy, *Appl. Phys. Lett.* **104**, 263701 (2014).
- [10] J. Zhao, J. Wu, and S. Yan, Erection mechanism of glossal hairs during honeybee feeding, *J. Theor. Biol.* **386**, 62 (2015).
- [11] K. C. Richardson, R. D. Wooller, and B. G. Collins, Adaptations to a diet of nectar and pollen in the marsupial *Tarsipes rostratus* (Marsupialia: Tarsipedidae), *J. Zool.* **208**, 285 (1986).
- [12] J. Seiwert, C. Clanet, and D. Quéré, Coating of a textured solid, *J. Fluid Mech.* **669**, 55 (2011).
- [13] A. Nasto, M. Regli, P.-T. Brun, J. Alvarado, C. Clanet, and A. E. Hosoi, Air entrainment in hairy surfaces, *Phys. Rev. Fluids* **1**, 033905 (2016).
- [14] E. Guyon, *Physical Hydrodynamics* (Oxford University Press, New York, 2001).
- [15] J. F. Swindells, *Viscosities of Sucrose Solutions at Various Temperatures: Tables of Recalculated Values* (US GPO, Washington, DC, 1958), Vol. 440.
- [16] C. Zhao, J. Wu, and S. Yan, Observations and temporal model of a honeybee's hairy tongue in microfluid transport, *J. Appl. Phys.* **118**, 194701 (2015).
- [17] C. Ishino, M. Reyssat, E. Reyssat, K. Okumura, and D. Quere, Wicking within forests of micropillars, *Europhys. Lett.* **79**, 56005 (2007).